CHAPTER 4
ENHANCED GAS ADSORPTION IN BERYLIUM, BORON, AND ALUMINIUM DOPED α-CN

4.1.INTRODUCTION

In the past, researchers have explored 2D monolayer of α-CN as a potential candidate for CO, NO and NH_3 sensing applications due to the lethality of these hazardous gases on the living organisms[1,2,3]. However the results are not that appreciative in terms of adsorption energies and distances.[4],[5] The underlying reason is perhaps the wide band gap of 3.8 eV in case of pristine monolayer[6], which is roughly three times the requisite 1.23 eV for gas sensing applications. Nevertheless, doping serves to notably diminish this gap, rendering it conducive to gas sensing purposes: a transition similar to the shift from intrinsic to extrinsic behavior. Moreover, studies reveal that the impurity doping in the 2D monolayers leads to the enhancement in the gas sensing performances. For instance, the doping of P-block elements in $MoTe_2$[1], doping of Ag, Au in HfS_2[7], and Au-doping in WSe_2[8] monolayers yield the improved CO adsorption performance. A study by Luo et al explores enhancement of NO adsorption by B, Al, Si, and S atoms on the BP monolayer and also capturing of NH_3 and NO_2 gas molecule by MoS_2 monolayer doped with Al, Si and P atoms [2]. According to a work by Ma et al, Au, Ni, Pd, and Pt doping improves adsorption performance of MoS_2 monolayer towards CO and NO gases [9]. Yong et al. studied C_2N monolayer for NH_3 and NO sensor and they observed that C_2N monolayer is a promising candidate with a small recovery time (1.2ms and 23μs for NH_3 and NO) at room temperature[5]. Hadi et al. reported the adsorption energy of g-CN can be increased up to -4.47 eV through Ir-embedding [10].

Following the previous chapter, in this chapter we have revisited the monolayer α-CN with different dopants. Here we have examined the adsorption of CO, NO, and NH_3 molecules over the monolayers doped with Beryllium (Be), Boron (B), and Aluminum (Al). The impurity atoms were chosen because they are similar in size to C and N atoms. The α-CN monolayer has two possible sites for substitutional doping: C-site and N-site, out of which we employed the C-site for further calculations for Al atom as it is the trivalent impurity. For B and Be atoms, we have chosen both C- and N-sites given the fact they are similar in size as compared to both carbon and nitrogen. This yields six potential configurations for each gas molecule (C-site Be and B doped α-CN, N-site B doped α-CN, and C-site Al doped α-CN)[11,12]. Our objective is to identify the most suitable candidate for gas sensing or removal applications among these configurations. In addition to analyzing the structural properties of doped α-CN monolayers, such as lattice parameter; adsorption properties such as adsorption energy, Löwdin population charge analysis, and electronic properties such as band structure and projected density of states (PDOS) before and after CO,

NO, and NH_3 gas adsorption, this study also explores sensing properties like work function and recovery time.

4.2.METHODOLOGY

For the analysis of electronic and structural properties of α-CN, Quantum Espresso simulation package [13] was used employing *first principles*-based density functional theory (DFT) calculation [14]. Electron exchange and correlation energies were calculated using generalized gradient approximation (GGA) in the form of Perdew-Burke-Erenzerhof (PBE)[15] Van der Waals interactions were embedded between α-CN and gas molecules and for the execution of precise results, the DFT-D2 method of Grimme has been employed. To perform all the calculations at the lowest cutoff energy we used plan-wave ultrasoft pseudopotential[16]. The value of kinetic energy cutoff for wave function was set to 80 Ry, which was sufficient for the fully convergence of total energy and structural parameters within the specified threshold criterion. The Brillouin zone integration was sampled by using the Monkhorst-pack scheme[17] having 8×8×1 k-point mesh. The vacuum space between two consecutive layers was set to 22 Å in order to avoid interactions between layers in nearest neighbour unit cells. The atomic structure symmetry was fixed and all atomic positions of an atoms were fully relaxed until the maximum residual forces on each atom is less than 0.001 eV/Å. For the visualization of fully relaxed geometrical structure Xcrysden software was used[18].

We have taken into account 3×3×1 supercell of α- CN containing 36 atoms for the investigation of adsorption properties. For the calculation of adsorption energy, we have used the following equation[19]

$$E_{ads} = E_{\alpha-\mathrm{CN+Gas}} - (E_{\alpha-\mathrm{CN}} + E_{Gas}) \qquad (1)$$

Where $E_{\alpha-\mathrm{CN+Gas}}$ is the total energy of gas adsorbed α- CN monolayer, $E_{\alpha-\mathrm{CN}}$ is the total energy of α- CN monolayer and E_{Gas} is the total energy of isolated gas molecules. A negative adsorption energy value signifies an exothermic process, indicating the stable adsorption of the gas molecule onto the monolayer system.

4.3. RESULTS AND DISCUSSION

4.3.1. Physical and Electronic Characteristics of Beryllium, Boron and Aluminium doped α-CN Monolayer

Before delving into the adsorption investigation, the B, Be and Al doped α-CN underwent geometry optimization. The illustration in Figure 4.1(a), 4.2(a) and 4.3(a) portrays the optimized configuration of α-CN monolayer doped with Be, B and Al.

We have investigated the potential of using Beryllium (Be) as a dopant. As discussed in Section 4.1, we identified two possible doping sites: the C site and the N site. Figures 4.1 (a) and (d) show the optimized structures of Be-doped α-CN at the C site and N site, respectively. Doping with Be results in significant modifications to the lattice parameter of α-CN, with an increase of 0.84% observed for Be doped at the C site and 1.26% for Be doped at the N site. These structural changes have a profound impact on the electronic properties of the material. Specifically, Be doping at the C site results in a decrease in the bandgap (Figure 4.1(b)). In the case of Be-doped α-CN at the N site, there is an observed overlap of C-2p, Be-2p, and C-2s orbitals at the Fermi level.

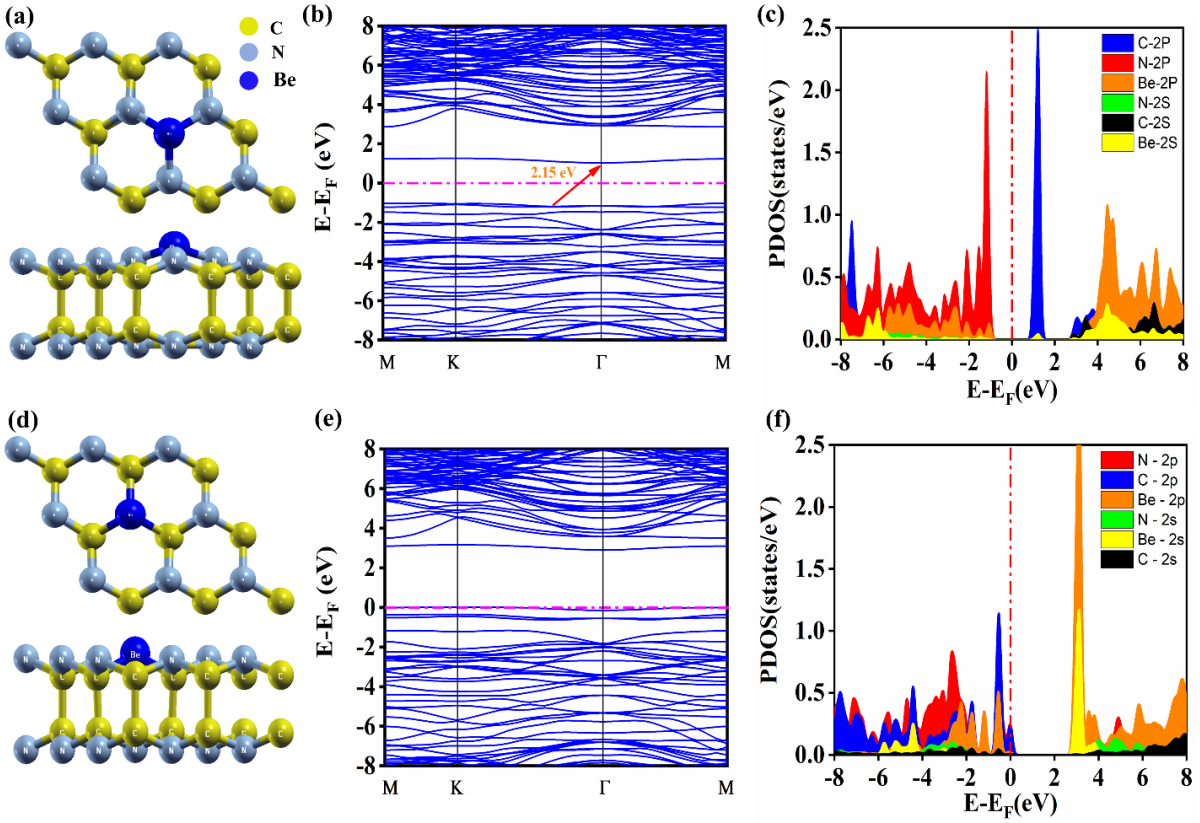

Figure 4.1: Optimized geometries, band structure and PDOS plots for Be doped α-CN at C site (a, b, c) and Be doped α-CN at N site (d, e, f)

To enhance the adsorption capabilities of pristine α-CN, Boron atoms were also doped at two potential sites: the C site and the N site. Figures 4.2 (a) and (d) display the optimized geometric structures of boron-doped α-CN at the C site and N site, respectively. This doping results in changes to the lattice parameter, with an observed increase of 0.4% for boron doped at the C site and 0.8% for boron doped at the N site, as shown in Table 4.1. These structural modifications lead to alterations in the electronic properties of the material. For boron doping at the C site, there is an overlap of bands at the Fermi level, as depicted in Figure 4.2(b), and further confirmed by the partial density of states (PDOS) projections of C-2p, C-2s, and B-2s orbitals, shown in Figure 4.2 (c). In the case of boron doping at the N site, a reduction in the bandgap from 3.71 eV[20] to 1.56 eV is observed. This decrease in bandgap value increases the system's conductivity, which is crucial for gas sensing applications, as illustrated in Figures 4.2 (e) and (f).

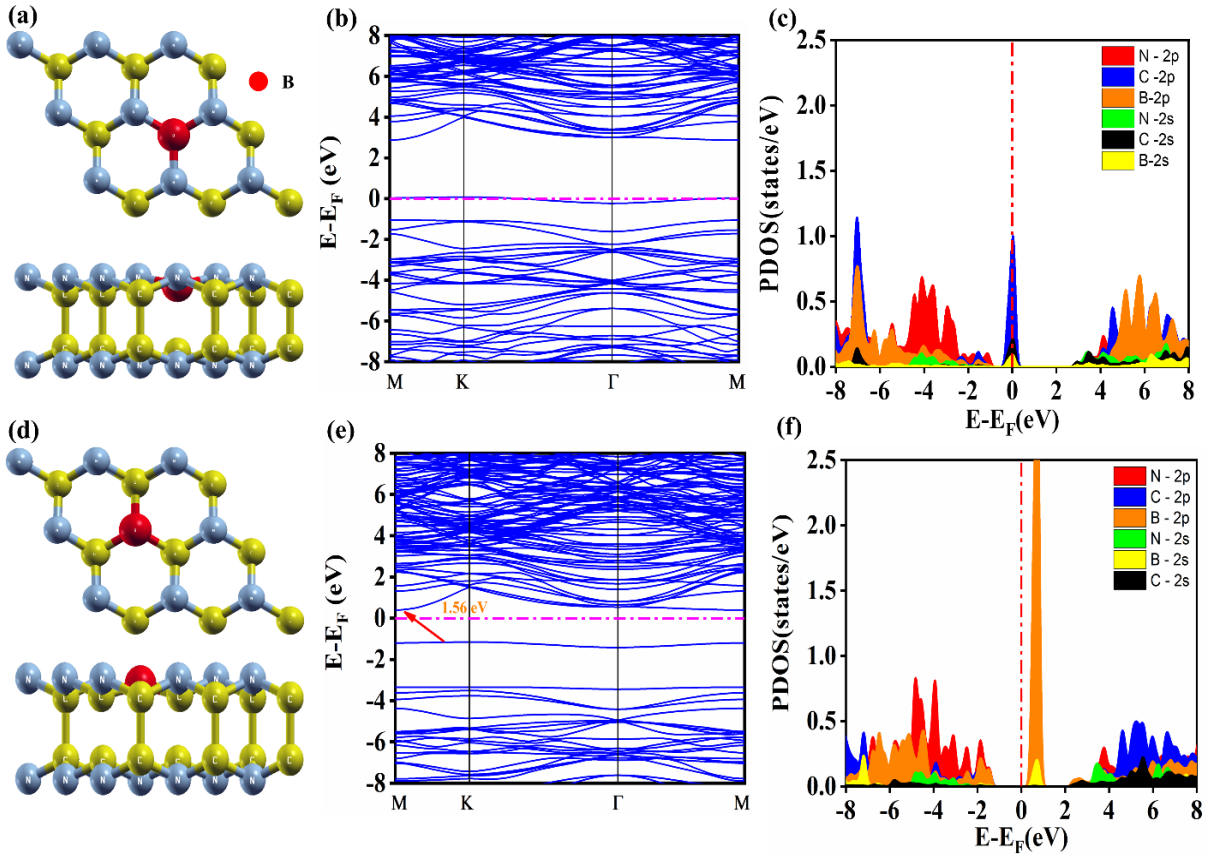

Figure 4.2: Optimized geometries, band structure and PDOS plots of B doped α-CN at C site (a, b, c) and B doped α-CN at N site (d, e, f) respectively.

Doping of Aluminium induces structural variations in the material as well. Minor changes are observed in the C-C, C-N, and N-N bond lengths before and after functionalization. In α-CN, the bond angles (C-C-N and C-N-C) decrease following Al-doping. Additionally, the lattice parameters of α-CN slightly increase by 0.01 Å after Al-doping, attributed to the larger atomic radius of the Al atom. These structural changes lead to alterations in the electronic properties of the system. Consequently, the material becomes an extrinsic semiconductor with overlapping Al-3s, N-2p, N-2s, and Al-3p orbitals at the Fermi level.

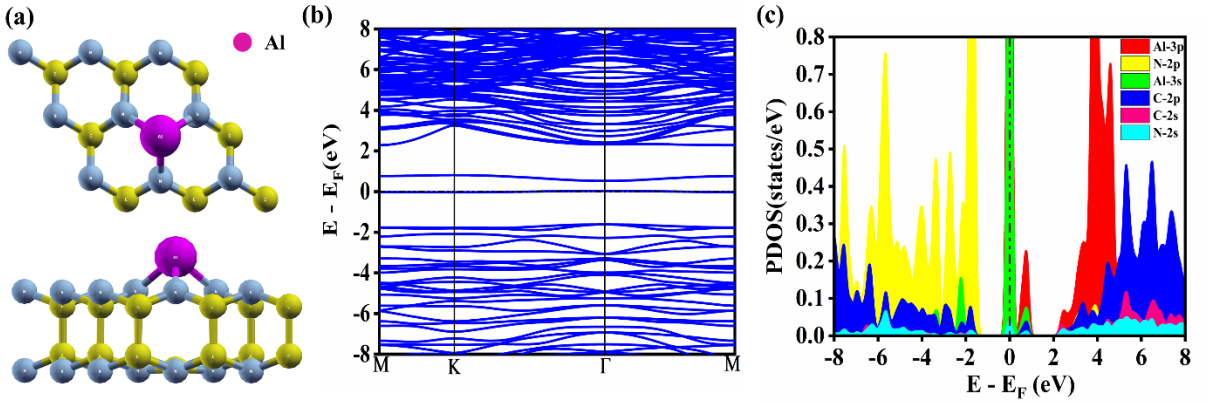

Figure 4.3: Optimized geometries, band structure and PDOS plots of Al doped α-CN at C site (a, b, c)

4.3.2. Adsorption performance of CO, NO and NH_3 gas molecules on Be doped α-CN

Following Be doping, three potential sites were considered for the adsorption of gases, i.e. top of C, top of N and top of dopant. Subsequently, for further calculations, we have taken into account a most stable structure with the minimum energy value. Adsorption of CO gas molecules on Be-doped α-CN at C site, with the adsorption energy value (E_{ads}) of -0.49 eV results in slight diminution of energy band gap value, which indicates intensification of electrical conductivity. The low adsorption energy value suggests predominantly Van der Waals interactions between the CO gas molecule and the system. (See fig 4.4 (a), (b), (c)). For Be doped α-CN at N site, formation of covalent bond takes place between the system and CO gas molecules with the E_{ads} = -1.38 eV. (See Table 4.1). It is also noticeable from the hybridization of C-2p, Be-2p, and C-2s orbitals on Fermi level in partial density of states (pdos). (See Fig 4.4 (f)).

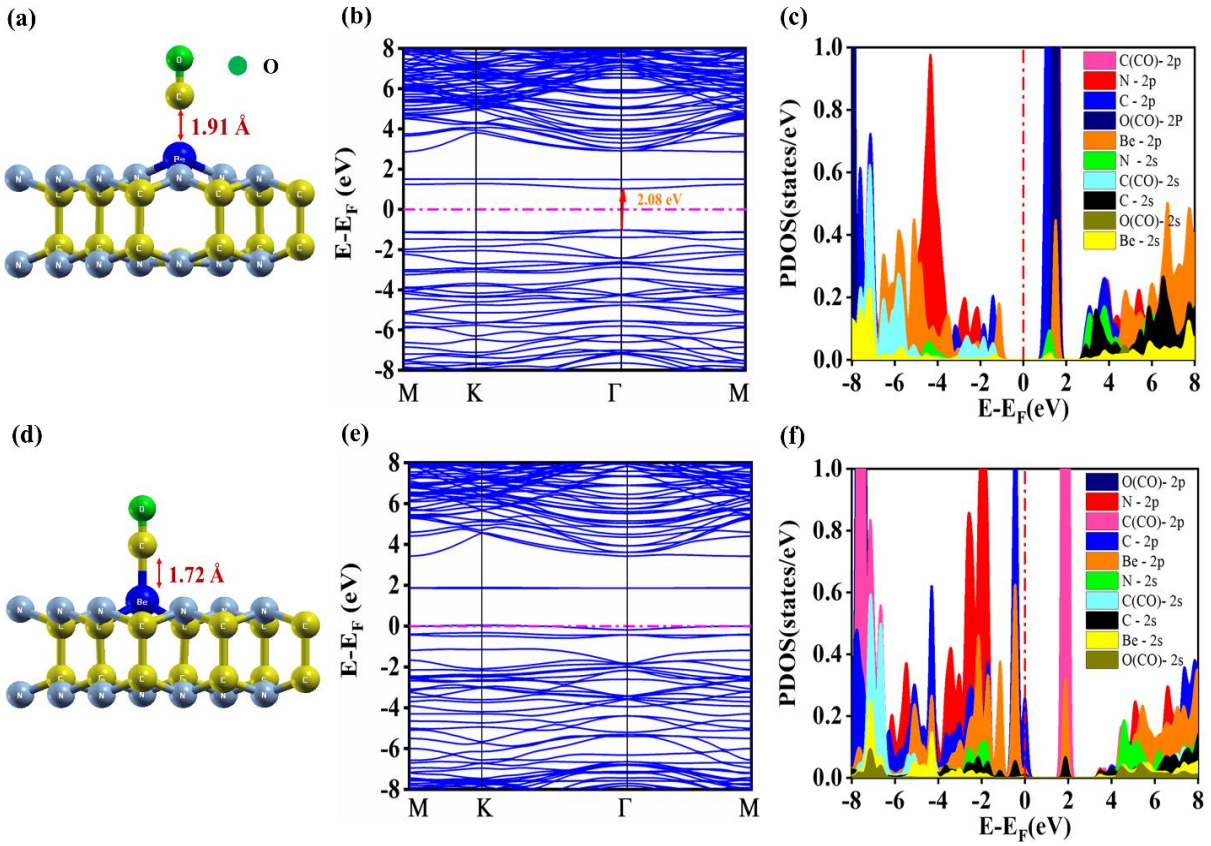

Figure 4.4: Minimum energetic configurations, band structure and PDOS plots of CO adsorbed on Be doped α-CN at C site (a, b, c) and Be doped α-CN at N site (d, e, f)

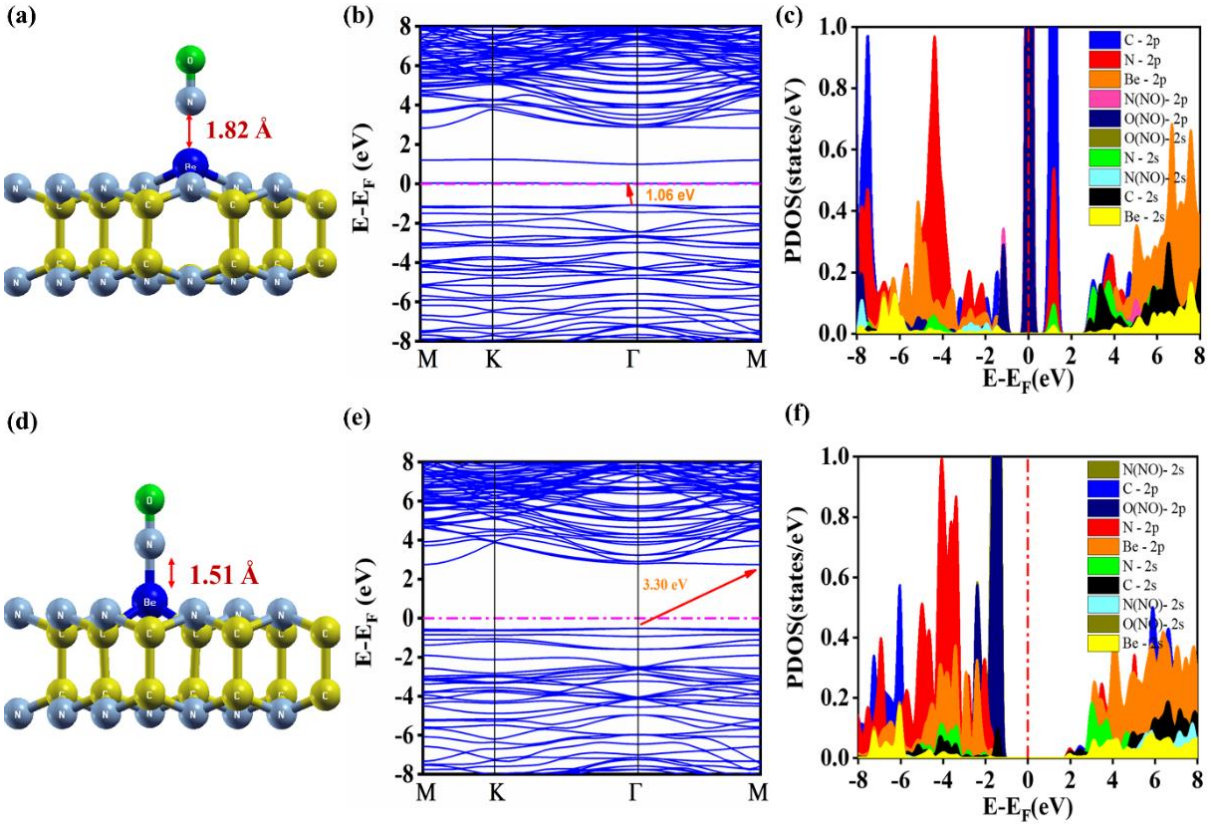

Figure 4.5: Minimum energetic configurations, band structure and PDOS plots of NO adsorbed on Be doped α-CN at C site (a, b, c) and Be doped α-CN at N site (d, e, f)

The interaction of NO gas molecules with Be-doped α-CN exhibits distinct behaviours depending on whether the doping occurs at the carbon (C) or nitrogen (N) sites. Specifically, when Be is doped at the C site, the NO gas molecules undergo physisorption with the α-CN monolayer. This is characterized by a low adsorption energy value signifying a weaker interaction, and a minimal charge transfer between the gas molecules and the monolayer. These details can be observed in Table 4.2 and Table 4.4, which highlight the adsorption energy and charge transfer values respectively. On the other hand, when Be is doped at the N site, the adsorption of NO gas does not result in significant changes in the electronic properties of the α-CN system. This is evidenced by the lack of observable modifications in the energy band gap or electrical conductivity of the material. Consequently, the system's overall nature remains unchanged despite the presence of the NO gas molecules. This lack of significant interaction implies that doping Be at the N site does not enhance the sensitivity or reactivity of α-CN towards NO gas molecules.

Table 4.1: Structural parameter, adsorption energy, adsorption distance, electronic bandgap of Beryllium doped α-CN with gas molecule

System		Bond length (Å)				Angle (º)	d (Å)	E_{ads} (eV)	E_g (eV)
		C-C	N-N	Be-N	Be-C				
Be doped at C site	Before adsorption	--	2.64	1.53	3.02	$74.89^{(C\text{-}Be\text{-}N)}$ $119.96^{(Be\text{-}N\text{-}C)}$	--	--	
	CO	--	2.65	1.58	3.19	$68.02^{(C\text{-}Be\text{-}N)}$ $121.88^{(Be\text{-}N\text{-}C)}$	1.91	-0.49	2.08
	NO	--	2.69	1.58	3.20	$67.76^{(C\text{-}Be\text{-}N)}$ $121.96^{(Be\text{-}N\text{-}C)}$	1.82	-0.32	1.06
	NH_3	--	2.70	1.60	3.25	$65.97^{(C\text{-}Be\text{-}N)}$ $122.47^{(Be\text{-}N\text{-}C)}$	1.80	-1.23	-
Be doped at N site	Before adsorption	1.59	--	2.75	1.61	$104.53^{(C\text{-}Be\text{-}C)}$ $111.07^{(C\text{-}C\text{-}Be)}$	--	--	
	CO	1.62	--	2.86	1.65	$100.02^{(C\text{-}Be\text{-}C)}$ $115.03^{(C\text{-}C\text{-}Be)}$	1.72	-1.38	-
	NO	1.63	--	2.92	1.69	$98.42^{(C\text{-}Be\text{-}C)}$ $115.73^{(C\text{-}C\text{-}Be)}$	1.51	-1.48	3.30
	NH_3	1.62	--	2.87	1.66	$99.39^{(C\text{-}Be\text{-}C)}$ $115.93^{(C\text{-}C\text{-}Be)}$	1.71	-2.18	-

In the case where α-CN is doped with beryllium (Be) at the carbon (C) site, the adsorption of an NH_3 gas molecule occurs through physisorption, meaning there is no bond formation and the adsorption distance is 1.80 Å (as shown in Fig. 4.6(a)). This indicates that Van der Waals forces are responsible for the interaction between the α-CN system and the NH_3 gas molecule. Conversely, when α-CN is doped with Be at the N site, chemisorption takes place. This involves the formation of a covalent bond between the system and the NH_3 gas molecule, as illustrated in Fig. 4.6(d). The presence of this covalent bond signifies a stronger and more specific interaction compared to physisorption. Furthermore, the projected density of states (PDOS) analysis reveals significant hybridization between the N(NH_3)-2p, C-2p, Be-2p, N-2p, C-2s, and N-2s orbitals at the Fermi level (depicted in Fig. 4.6(f)). This hybridization, along with a substantial charge transfer between the system and the NH_3 gas molecules, supports the observation of chemisorption when Be is doped at the N site.

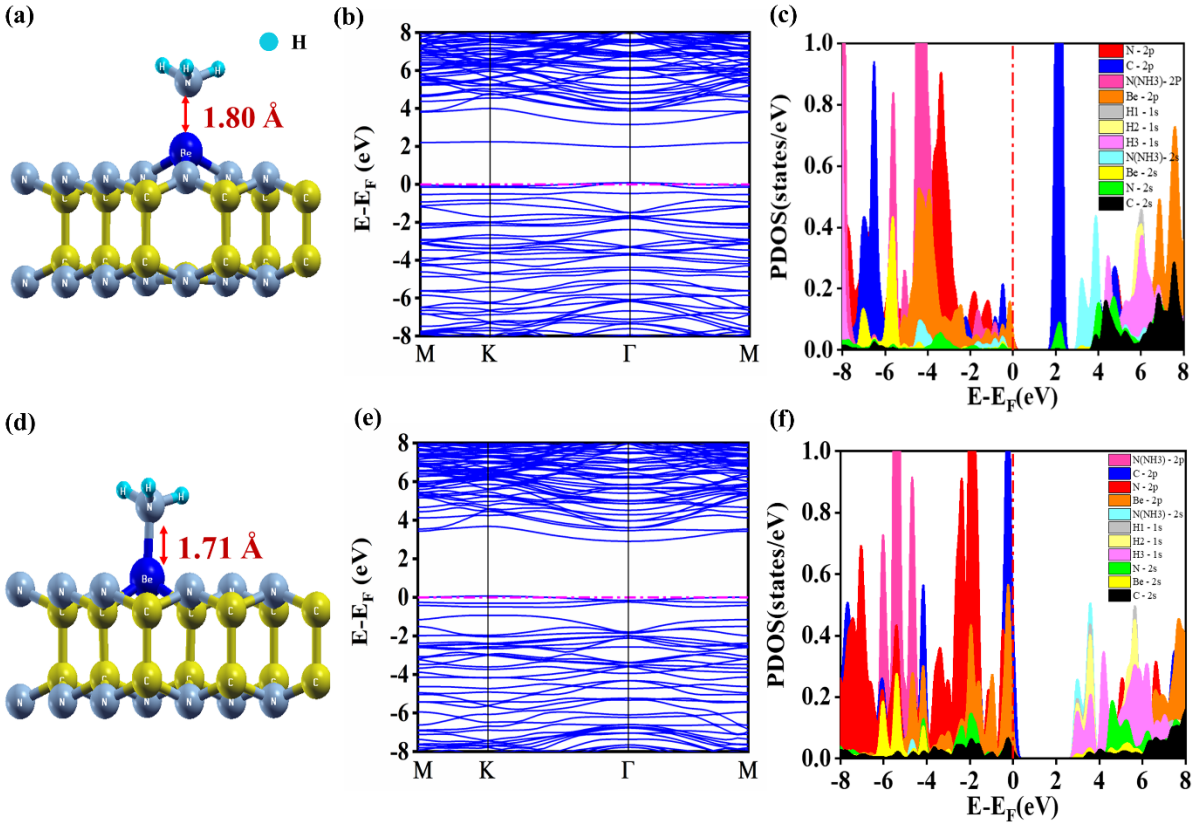

Figure 4.6: Minimum energetic configurations, band structure and PDOS plots of NH_3 adsorbed on Be doped α-CN at C site (a, b, c) and Be doped α-CN at N site (d, e, f)

4.3.3. Adsorption performance of CO, NO and NH_3 gas molecules on B doped α-CN

The adsorption of CO gas on B-doped α-CN at the C site exhibited an E_{ads} value of -0.10 eV, with an adsorption distance of 3.23 Å, indicative of a weak interaction between the CO molecule and the system. (Fig 4.7 (a),(b), (c)).Conversely, when CO gas adsorbed on B-doped α-CN at the N site, a small adsorption distance of 1.56 Å was observed alongside a significantly higher E_{ads} value of -1.38 eV. Formation of covalent bond between the gas molecule and the system demonstrates chemisorption. (Fig 4.7(d),(e),(f)) Quantitative analysis of charge transfer (Löwdin charge transfer) indicates a transfer of charge from the CO gas molecule to the system, providing justification for this observation. (Table 4.4)

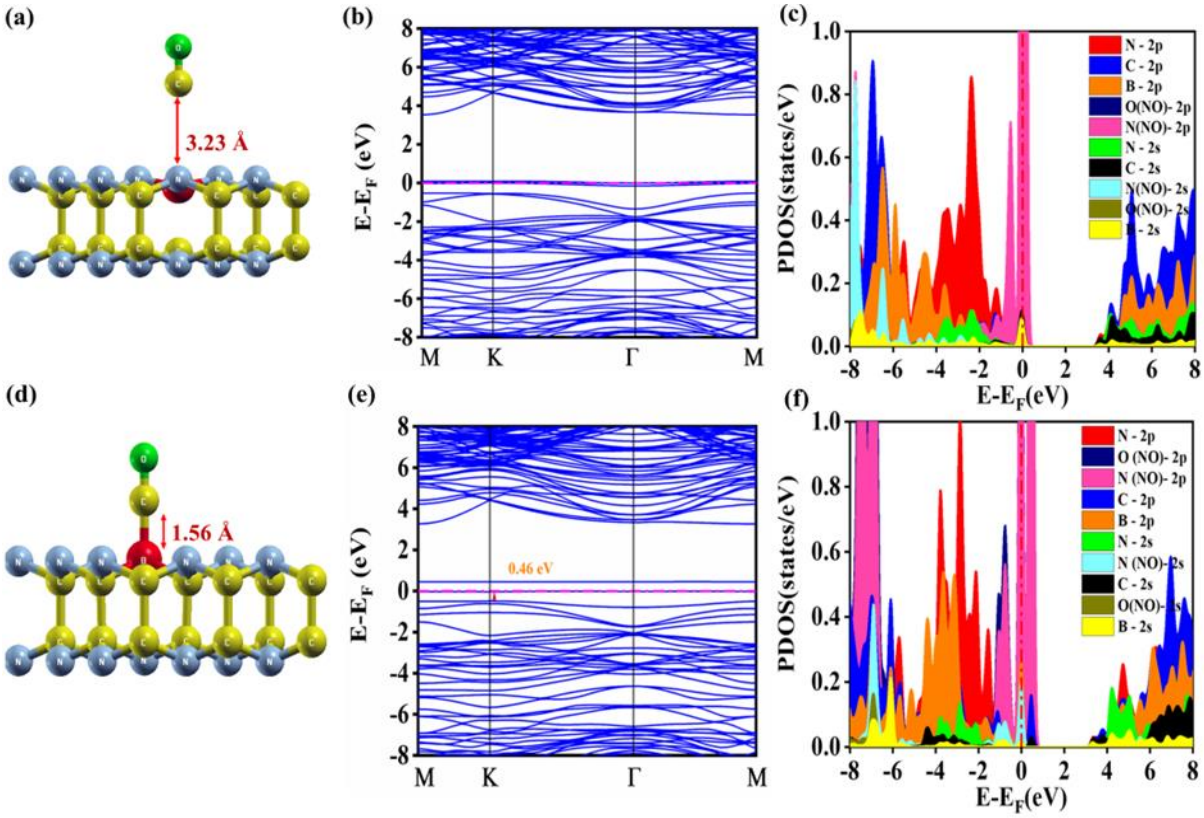

Figure 4.7: Minimum energetic configurations, band structure and PDOS plots of CO adsorbed on B doped α-CN at C site (a, b, c) and B doped α-CN at N site (d, e, f)

In the scenario where NO gas molecules adsorb onto B-doped α-CN at the carbon (C) site, the interaction between the gas molecule and the system is characterized by a lack of bond formation. This results in a large adsorption distance, indicative of a weak interaction between the NO gas and the α-CN monolayer. The considerable separation between the gas molecule and the doped system highlights the minimal influence the gas has on the material when doped at the C site. Conversely, when boron (B) is doped at the N site of α-CN, the adsorption behaviour changes significantly. The adsorption energy (E_{ads}) value is noted to be –1.75 Å, which suggests a much stronger interaction. Furthermore, the projected density of states (PDOS) analysis reveals notable hybridization involving multiple orbitals: N(NO)-2p, N(NO)-2s, B-2s, C-2p, B-2p, and C-2s at the Fermi level. This hybridization indicates a substantial electronic interaction between the gas molecule and the doped α-CN system. As a result of this significant orbital hybridization, the doped system undergoes a transition to become an extrinsic semiconductor. This transformation is accompanied by chemisorption, where a chemical bond forms between the NO gas molecule and the B-doped α-CN at the N site. This chemisorption process highlights the strong and specific interaction between the gas and the doped material, contrasting sharply with the weak physisorption observed at the C site.

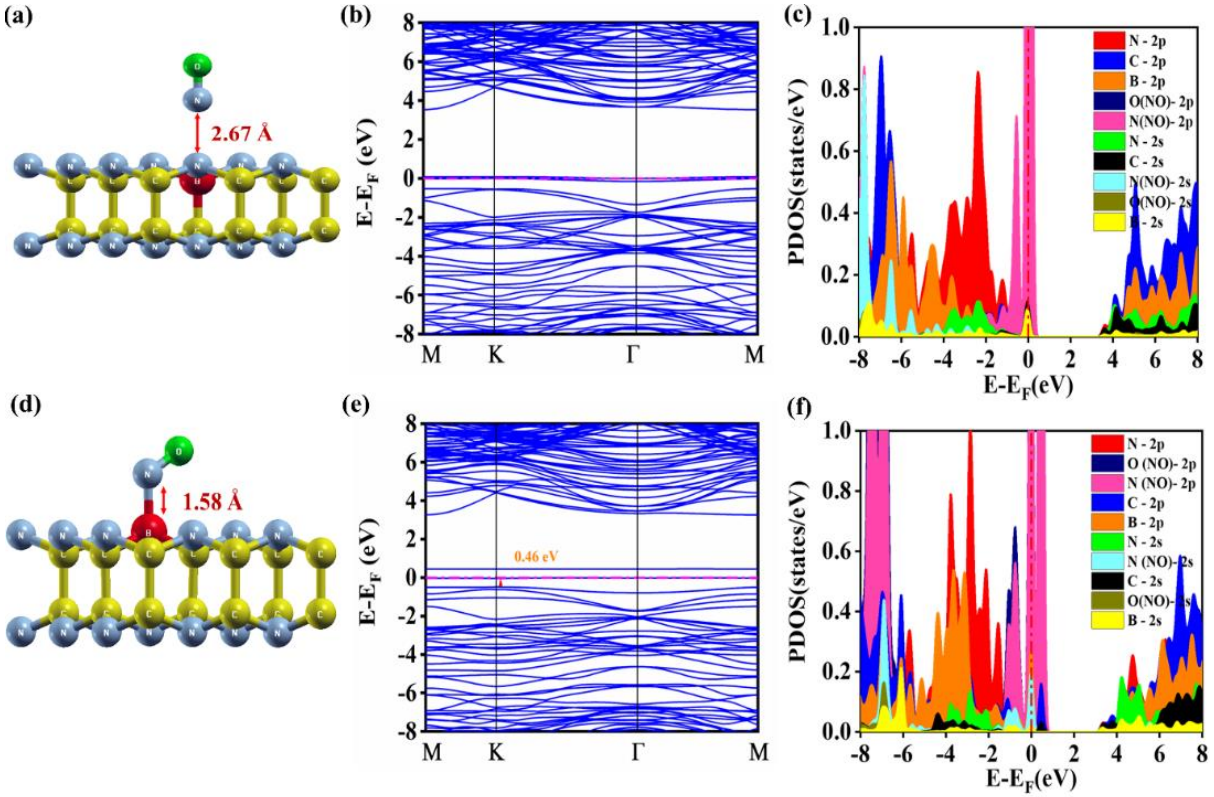

Figure 4.8: Minimum energetic configuration, band structure and PDOS plots of NO adsorbed B-doped (at C site) α-CN (a, b, c) and B-doped (at N site) α-CN (d, e, f)

In addition, the adsorption of NH_3 gas on B-doped α-CN exhibits contrasting behaviours depending on whether the doping occurs at the carbon (C) site or the nitrogen (N) site. When NH_3 gas interacts with B-doped α-CN at the C site, the E_{ads} value is notably low, indicating a weak interaction. The NH_3 gas molecule acts as a charge acceptor in this scenario, with a charge transfer of 0.35 electrons from the α-CN system to the gas molecule. This minimal charge transfer and low adsorption energy highlight the weak physisorption nature of the interaction at the C site. (Figure 4.9 (a),(b),(c)).In contrast, when B is doped at the N site of α-CN, the interaction with NH_3 gas is markedly stronger, resulting in chemisorption. This is evidenced by a significantly higher E_{ads} value of -2.89 eV and a much shorter adsorption distance of 1.58 Å. The stronger interaction at the N site is further corroborated by the projected density of states (PDOS) analysis. The PDOS reveals substantial hybridization among the N(NH_3)-2s, H-2s, N-2p, C-2p, and N-2s orbitals at the Fermi level. This hybridization suggests a more significant electronic interaction and bond formation between the gas molecule and the doped system. (See Fig 4.9 (f))

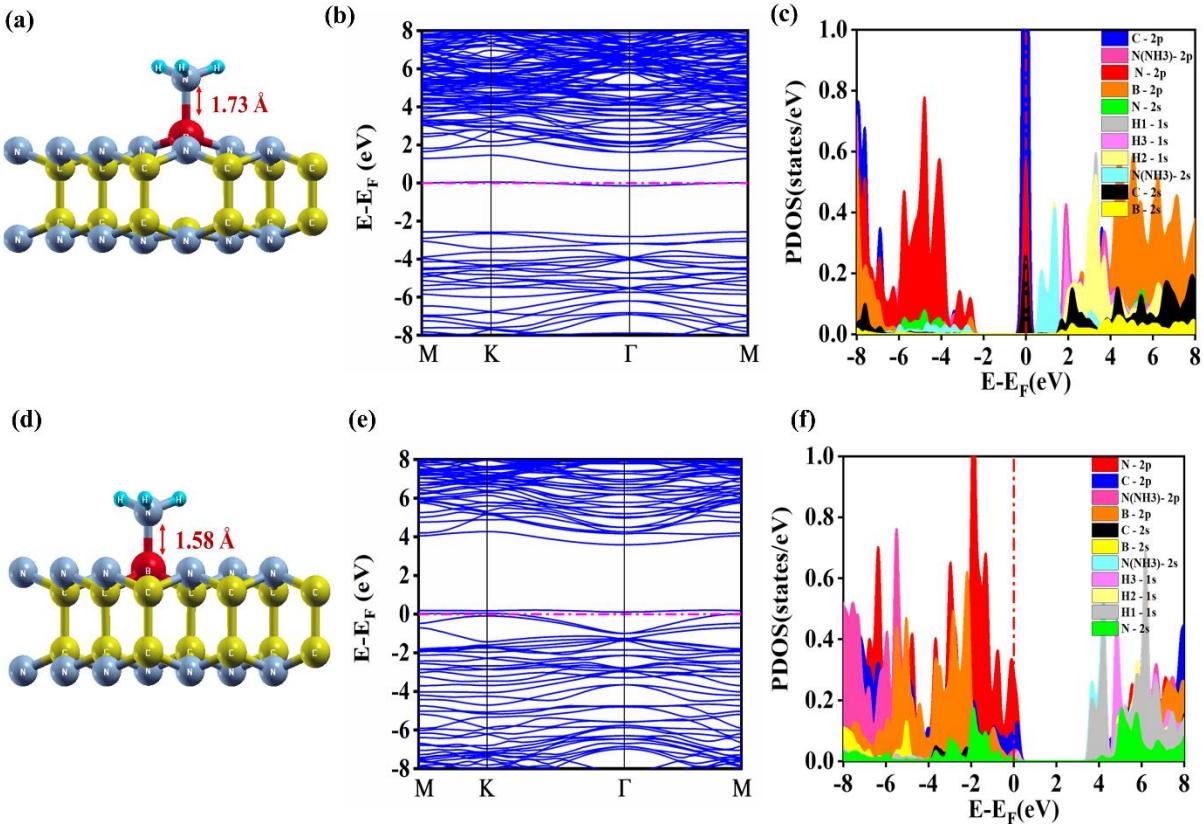

Figure 4.9: Minimum energetic configuration, band structure and PDOS plots of NH_3 adsorbed B-doped (at C site) α-CN (a, b, c) and B-doped (at N site) α-CN (d, e, f)

Table 4.2: Structural parameter, adsorption distance, adsorption energy, electronic bandgap of Boron doped α-CN with gas molecule

System		Bond length (Å)				Angle (º)	d (Å)	E_{ads} (eV)	E_g (eV)
		C-C	N-N	B-N	B-C				
B doped at C site	Before adsorption	--	2.65	1.45	2.01	$100.01^{(C-B-N)}$ $112.22^{(B-N-C)}$	--	--	-
	CO	--	2.65	1.45	1.99	$100.23^{(C-B-N)}$ $112.14^{(B-N-C)}$	3.23	-0.10	-
	NO	--	2.69	1.50	1.65	$109.39^{(C-B-N)}$ $108.16^{(B-N-C)}$	2.67	-0.26	-
	NH_3	--	2.70	1.49	2.85	$74.28^{(C-B-N)}$ $121.11^{(B-N-C)}$	1.73	-0.43	-
B doped at N site	Before adsorption	1.72	--	2.50	1.48	$116.24^{(C-B-C)}$ $99.17^{(C-C-B)}$	--	--	1.56
	CO	1.62	--	2.67	1.54	$107.41^{(C-B-C)}$ $109.53^{(C-C-B)}$	1.56	-1.79	1.69
	NO	1.63	--	2.69	1.54	$106.96^{(C-B-C)}$ $109.25^{(C-C-B)}$	1.58	-1.75	0.46
	NH_3	1.62	--	2.67	1.54	$106.94^{(C-B-C)}$ $110.26^{(C-C-B)}$	1.58	-2.89	-

4.3.4. Adsorption performance of CO, NO and NH_3 gas molecules on Al doped α-CN

For Aluminium doped α-CN, the most stable configuration is when a CO gas molecule adsorbs atop the Al atom. This adsorption process is characterized by E_{ads} of -0.88 eV and an adsorption distance of 2 Å, (See Table 4.3)which signifies the formation of a covalent bond, indicative of chemisorption. The projected density of states (PDOS) analysis provides clear evidence of this bonding interaction. It reveals overlapping orbitals at the Fermi level, specifically the C(CO)-2p, Al-3p, O-2p, and C-2s orbitals, which collectively demonstrate the bonding between the CO gas molecule and the α-CN surface. This comprehensive analysis is detailed in Figure 4.10 (a), (b), and (c).

Here, NO gas molecule is observed to adsorb on Al doped α-CN atom with even greater energy. The adsorption energy in this case is -1.89 eV, and the adsorption distance is measured at 1.77 Å. The optimized structure of this adsorption configuration, depicted in Figure 4.10 (a), clearly shows chemisorption, characterized by the formation of a covalent bond between the NO gas molecule and the Al-doped α-CN. This conclusion is further corroborated by the PDOS analysis, which reveals significant orbital overlapping at the Fermi level. The involved orbitals include O-2p, Al-3p, N-2p, N(NO)-2p, N(NO)-2s, and Al-3s,

underscoring the strong electronic interaction and bond formation. Additionally, the NO gas molecule acts as a charge acceptor, with a charge transfer (Δq) of -0.121 e. This indicates a notable transfer of electron density from the α-CN surface to the NO molecule, enhancing the stability of the adsorption configuration. (See Table 4.4)

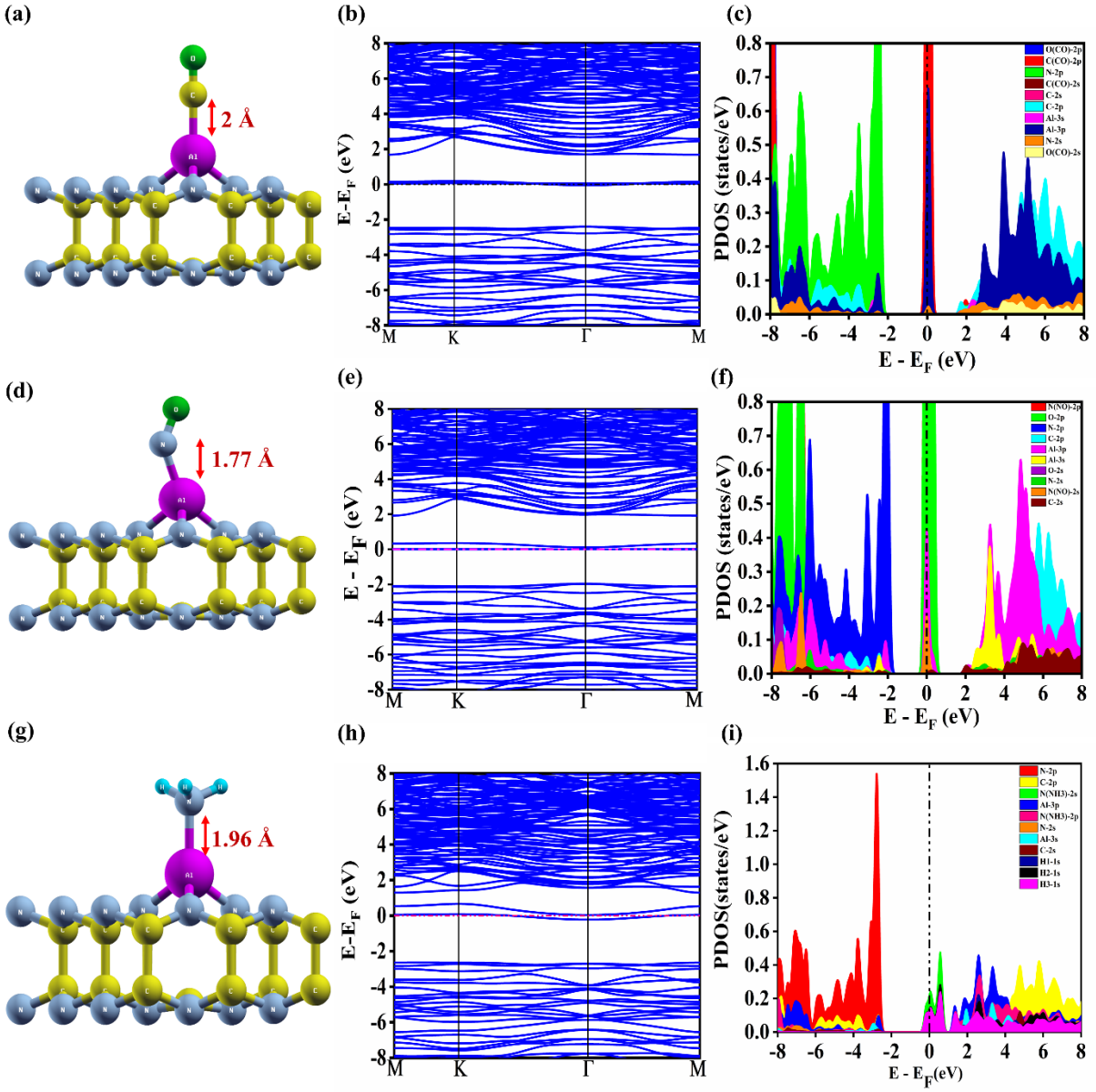

Figure 4.10: Minimum energetic configuration (a, d, g), band structure (b, e, h) and PDOS plots (c, f, i) of CO, NO and NH_3 gas molecules adsorbed on Al doped α-CN (at C site) respectively

NH_3 gas molecule adsorbs onto Al doped α-CN with an adsorption energy of -1.24 eV and an adsorption distance of 1.96 Å. This interaction leads to the formation of a covalent bond between the Al atom and NH_3 gas molecule. Additionally, PDOS plot reveals significant overlapping of Al-3p, H-1s and N(NH_3)-2s orbitals at the Fermi level. (See fig 4.10(i))This observation underscores the strong interaction and bond formation at the electronic level, contributing to the overall stability and electronic characteristics of the adsorbed system. The adsorption process is energetically favourable, as indicated by the negative adsorption energy. The relatively short adsorption distance suggests a strong interaction between the adsorbent and the adsorbate. The formation of a covalent bond between the Al atom in the doped α-CN and gas molecule is critical, as it affects the electronic properties of the material. The PDOS plot further illustrates the intricate electronic interactions taking place, showing how the orbitals of Al, H, and N contribute to the bonding and overall stability of the system.

Table 4.3: Structural parameter, adsorption energy, adsorption distance, electronic bandgap of Aluminium doped α-CN with gas molecule

System		Bond length (Å)				Angle (°)	d (Å)	E_{ads} (eV)	E_g (eV)
		C-C	N-N	Al-N	Al-C				
Al doped at C site	Before adsorption	--	2.62	1.86	2.86	$101.86^{(C\text{-}Al\text{-}N)}$ $123.47^{(Al\text{-}N\text{-}C)}$	--	--	-
	CO	--	2.62	1.80	2.82	$100.56^{(C\text{-}Al\text{-}N)}$ $123.23^{(Al\text{-}N\text{-}C)}$	2	-0.88	-
	NO	--	2.63	1.83	2.84	$103.87^{(C\text{-}Al\text{-}N)}$ $123.42^{(Al\text{-}N\text{-}C)}$	1.77	-1.89	-
	NH_3	--	2.62	1.77	2.79	$109.34^{C\text{-}Al\text{-}N)}$ $122.87^{(Al\text{-}N\text{-}C)}$	1.96	-1.24	-

Table 4.4: Löwdin charge transfer analysis

Gas molecule	System	Doping site	Löwdin charge (e) on atoms
CO		Isolated gas molecule	9.8307
	B doped α-CN	C site	9.8314
		N site	9.3767
	Be doped α-CN	C site	9.5462
		N site	9.4882
	Al doped α-CN	C site	9.8125
NO		Isolated gas molecule	10.8408
	B doped α-CN	C site	10.5149
		N site	10.7767
	Be doped α-CN	C site	10.6968
		N site	10.6119
	Al doped α-CN	C site	11.037
NH_3		Isolated gas molecule	7.8456
	B doped α-CN	C site	7.493
		N site	7.3974
	Be doped α-CN	C site	7.5977
		N site	7.5723
	Al doped α-CN	C site	7.8874

4.3.5. Work function Analysis

In the study of gas adsorption, it becomes imperative to examine the impact on crucial parameters such as the Fermi level and work function (ϕ) of the material. This is particularly significant in the context of ϕ-type sensors, where the estimation of work function values before and after gas adsorption operations is essential. A Kelvin oscillator instrument is commonly employed in these sensors to gauge ϕ-values. The gate voltage is modulated in response to changes in the work function induced by gas adsorption, generating an electrical signal. Defined as the minimum energy required to transfer an electron from a material to a location just outside its surface in a vacuum[21], the work function (ϕ) is a critical parameter in understanding material behaviour in gas sensing applications[22]

$$\varphi = E_{vac} - E_F \qquad (2)$$

In equation (2), where E_{vac} represents the vacuum energy level and E_F denotes the Fermi energy, it is observed that when E_{vac} equals 0, φ can be expressed as $-E_F$. The alteration in φ value within an adsorbent system due to gas adsorption significantly impacts its field emission properties, a relationship that can be elucidated through the classical Richardson-

Dushman equation. This equation provides a means to correlate the field emission current density for electrons in a vacuum[23]

$$j = AT^2\exp(-\varphi/kT) \qquad (3)$$

where A stands for Richardson constant (A/m^2) and T is the temperature.

Equation (3) indicates that the field emission current varies in inverse exponential proportion with respect to the work function. Which implies that the system which has considerable change in ϕ upon adsorption, will make a good candidate for work function based (ϕ- type) sensor. Table 4.5 presents the calculated work function values before and after adsorption. The work function plots[24],provide a parallel narrative to the interpretation presented in Table 4.5. Figure 4.11 illustrates the work function variations pre- and post-gas adsorption for both doping sites in the case of Be-doping. Likewise, Figures 4.12 and 4.13 showcases work function plots for B-doping, and Al doping, delineating changes before and after adsorption respectively. These visual representations help us understand how the work function values change with the adsorption of gas molecule on the system, giving us important information about the surface behaviour of the system and electronic properties of the doped material when exposed to gases.

Table 4.5: Work function analysis of Be, B and Al doped α-CN upon CO, NO and NH_3 adsorption

System	Doping Site	Before adsorption ϕ (eV)	After adsorption ϕ (eV)			Δϕ for adsorption		
			CO	NO	NH_3	CO	NO	NH_3
B doped α-CN	C-site	5.72	5.68	6.08	3.99	-0.69 %	6.29 %	-30.24 %
	N-site	5.22	5.56	6.20	6.82	6.51 %	18.77 %	30.65 %
Be doped α-CN	C-site	5.41	4.72	5.16	5.43	-12.75 %	-4.62 %	0.36 %
	N-site	6.22	4.90	4.72	6.03	-21.22 %	-24.11 %	-3.05 %
Al doped α-CN	C site	4.27	3.71	4.23	3.41	13.11 %	0.93 %	20.14 %

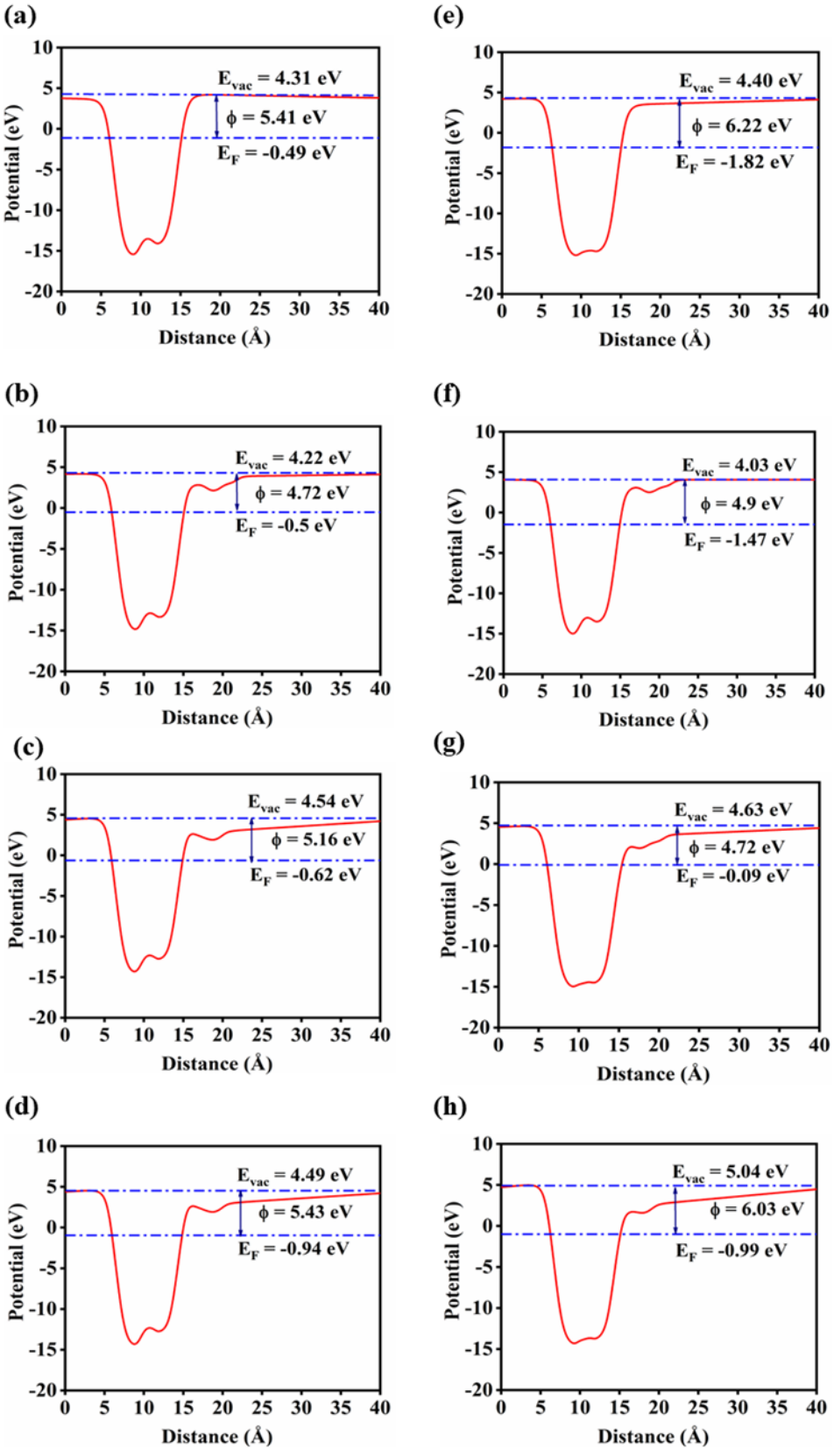

Figure 4.11: Work function plot of (a) Be doped α-CN at C side, adsorbed (b) CO gas (c) NO gas (d)NH_3 gas on Be doped α-CN at C site (e) Be doped α-CN at N site, adsorbed (f) CO gas (g) NO gas (h) NH_3 gas on Be doped α-CN at N site

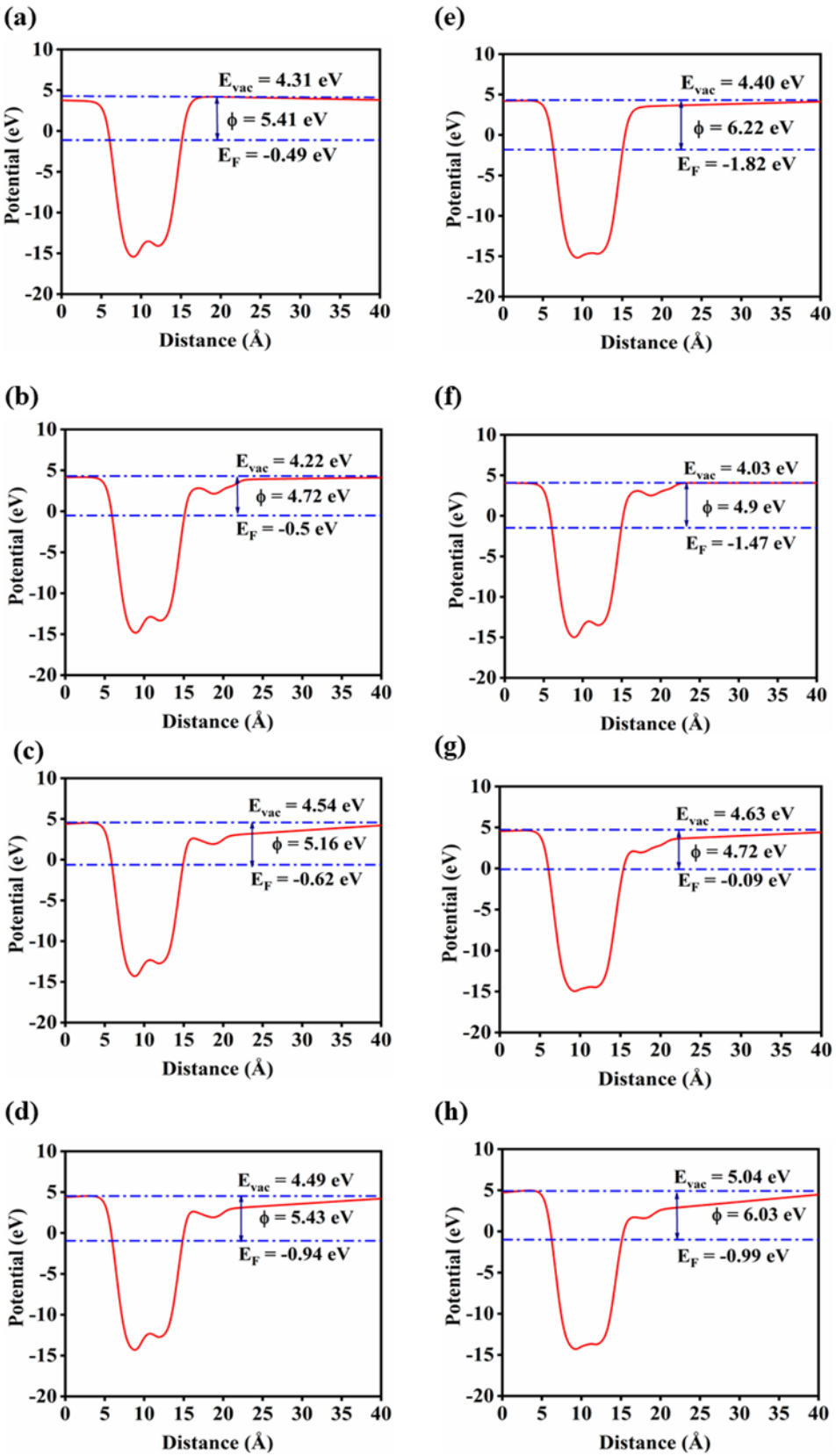

Figure 4.12: Work function plot of (a) B doped α-CN at C side, adsorbed (b) CO gas (c) NO gas (d) NH_3 gas on B doped α-CN at C site (e) B doped α-CN at N site, adsorbed (f) CO gas (g) NO gas (h) NH_3 gas on B doped α-CN at N site

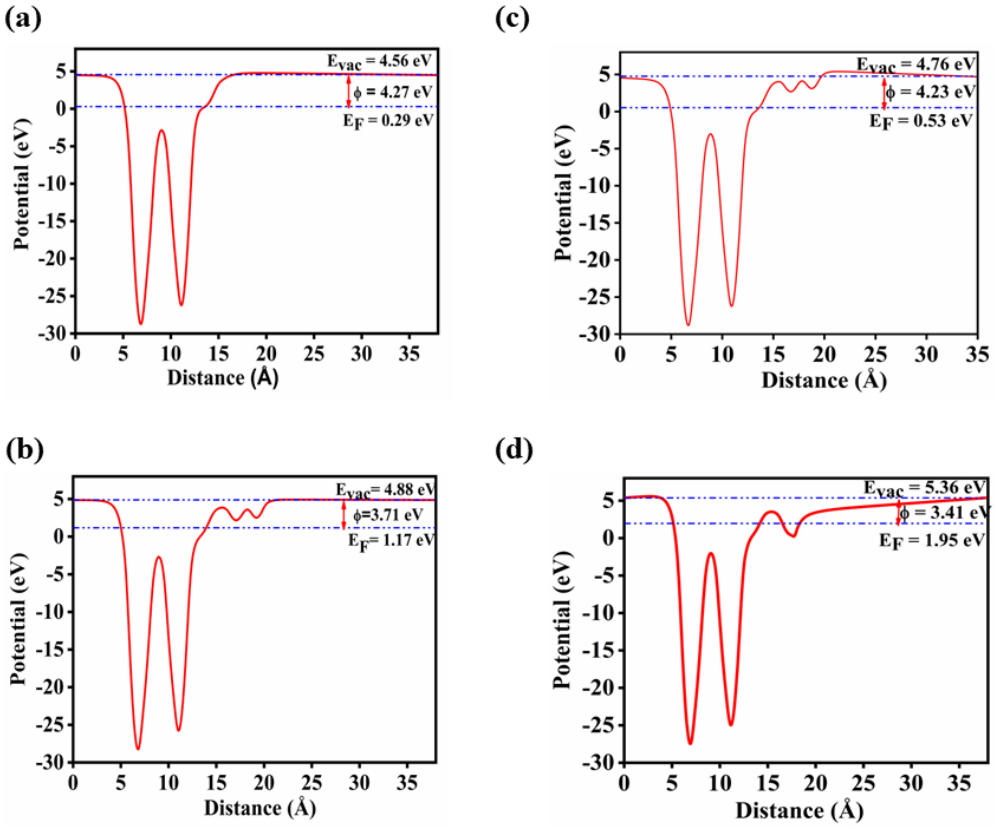

Figure 4.13: Work function plot of (a) Al doped α-CN at C side, adsorbed (b) CO gas (c) NO gas (d) NH_3 gas on Al doped α-CN at C site

Notably, significant alterations in the work function are observed upon CO gas molecule adsorption in the case of Be-doped α-CN at the N site, indicating a discernible impact on the system's conductivity after the adsorption. Furthermore, considering the NO gas molecule, the most substantial change in work function is detected in Be-doped α-CN at the N site, suggesting its potential suitability for ϕ-type sensors of NO gas molecules. Similarly, for NH_3 gas molecules, the highest change in work function occurs in B-doped α-CN at the C site, indicating its candidacy for NH_3 gas molecule detection. Therefore, Be-doped α-CN at the N site and B-doped α-CN at the N site are most suitable candidates for ϕ-type sensors of CO, NO gas and NH_3 gas respectively.

4.3.6. Recovery Time Analysis

For a gas sensor, the recovery time (τ) stands as a crucial parameter, representing the duration anticipated for the adsorbate to undergo self-desorption. Essentially, τ serves to outline the simplicity or complexity of the desorption process. Ideally, a sensor should exhibit a swift recovery time [34]. It is imperative for gas sensors to evade strong interactions with gases, as such interactions hinder the dissociation of gas molecules, thereby prolonging the desorption process and leading to longer recovery times. The formula governing τ is expressed as follows[25]

$$\tau = \upsilon^{-1} \exp\left(-\frac{E_{ads}}{KT}\right) \qquad (4)$$

To calculate τ, we have taken attempt frequency υ = 10^{12} s^{-1} (for IR radiation) and absolute temperature T = 300 K (see table 4.6).

In the case of NO gas molecule, for both B doping at the C site and Be doping at the N site, the computed recovery time is determined to be 10^{-7} seconds, which aligns optimally with the requirements for gas sensing applications but in the case of Al doped α-CN, the computed recovery time is notably prolonged, extending to several hours. Such extended recovery times renders it is suitable for NO gas removal applications from environment. In contrast, for CO and NH_3 gas molecules for Be doping at the N site and B doping at the N site, respectively again the long recovery time suggests it's application as a removal of toxic gas from the environment. On the contrary, B doped α-CN at both the C and N sites exhibits very small recovery times for CO adsorption, yet due to their minimal adsorption energies and substantial adsorption distances, they are unsuitable candidates for gas sensors.

Table 4.6. Recovery time for different gas adsorptions.

System	Gas molecule	Doping site	τ (s)
B-doped α-CN	CO	C-site	47.8×10^{-12}
		N-site	1.17×10^{18}
	NO	C-site	2.31×10^{-8}
		N-site	2.4×10^{17}
	NH_3	C-site	1.67×10^{-5}
		N-site	3.54×10^{36}
Be-doped α-CN	CO	C site	1.7×10^{-4}
		N site	1.52×10^{11}
	NO	C site	2.37×10^{-7}
		N site	7.30×10^{12}
	NH_3	C-site	4.61×10^{8}
		N-site	4.19×10^{24}
Al doped α-CN	CO	C site	06.30×10^{02}
	NO		08.11×10^{19}
	NH_3		6.78×10^{8}

4.4. Conclusion

In this chapter, we have calculated the structural, electronic, and sensing properties of Beryllium, Boron and Aluminium doped α-CN monolayers upon the adsorption of CO, NO, and NH_3 gas molecules. The substitutional doping of Be, B and Al atoms, causes some geometrical and electronic structure variations in the pristine α-CN monolayer. α-CN with Boron doping at C site is unsuitable for CO adsorption due to the large adsorption distance exceeding 3 Å. However, it proves suitable for NO and NH_3 sensing, as evidenced by optimal adsorption energies and distances. Conversely, for B doping at the N site and Al doping at C site are more suitable for removal applications, owing to highly negative adsorption energies and prolonged recovery times. Similarly, for Be doping at the C-site, α-CN demonstrates efficacy in removing all three gas molecules. The recovery time for NO adsorption over B doped α-CN at C site is on the order of nanoseconds, which registers its candidature for an "ultra-fast" sensor. From the work function analysis, we can conclude that B-doped α-CN at C-site as well at N-site is most suitable for a ϕ-type sensor in the case of NH_3 adsorption.

BIBLIOGRAPHY:

1 M. J. Szary, D. M. Florjan and J. A. Bąbelek, *ACS Sensors*, 2022, **7**, 272–285.

2 H. C. Luo, R. S. Meng, H. Gao, X. Sun, J. Xiao, H. Y. Ye, G. Q. Zhang and X. P. Chen, *IEEE Electron Device Lett.*, 2017, **38**, 1139–1142.

3 Y.-H. Zhang, Y.-B. Chen, K.-G. Zhou, C.-H. Liu, J. Zeng, H.-L. Zhang and Y. Peng, *Nanotechnology*, 2009, **20**, 185504.

4 H. Mistry, D. Chodvadiya, S. Vadalkar, K. N. Vyas and P. K. Jha, *Surfaces and Interfaces*, 2024, 46.

5 K. Bhattacharyya, S. M. Pratik and A. Datta, *J. Phys. Chem. C*, 2018, **122**, 2248–2258.

6 D. Chodvadiya, S. B. Pillai, B. Chakraborty and P. K. Jha, in *AIP Conference Proceedings*, American Institute of Physics Inc., 2020, vol. 2265.

7 G. Qian, W. Dai, F. Zhou, H. Ma, S. Wang, J. Hu and Q. Zhou, *Chemosensors*, 2022, **10**, 0–10.

8 X. Lu, L. Guo, P. Wang, M. Cui, D. Kanghong and W. Peng, *Appl. Surf. Sci.*, 2020, 513.

9 Z. Lu, P. Lv, D. Ma, X. Yang, S. Li and Z. Yang, *J. Phys. D. Appl. Phys.*, , DOI:10.1088/1361-6463/aaa3b3.

10 H. Basharnavaz, A. Habibi-Yangjeh and S. H. Kamali, *Mater. Chem. Phys.*, 2019, **231**, 264–271.

11 K. Zhang and J. Robinson, 2019, 1–24.

12 M. A. Rahman, *J. Asian Ceram. Soc.*, 2023, **11**, 215–224.

13 P. Giannozzi, S. Baroni, N. Bonini, M. Calandra, R. Car, C. Cavazzoni, D. Ceresoli, G. L. Chiarotti, M. Cococcioni, I. Dabo, A. Dal Corso, S. De Gironcoli, S. Fabris, G. Fratesi, R. Gebauer, U. Gerstmann, C. Gougoussis, A. Kokalj, M. Lazzeri, L. Martin-Samos, N. Marzari, F. Mauri, R. Mazzarello, S. Paolini, A. Pasquarello, L. Paulatto, C. Sbraccia, S. Scandolo, G. Sclauzero, A. P. Seitsonen, A. Smogunov, P. Umari and R. M. Wentzcovitch, *J. Phys. Condens. Matter*, 2009, **21**, 44.

14 W. Kohn, A. D. Becke and R. G. Parr, *Density Functional Theory of Electronic*

Structure, 1996.

15 J. P. Perdew and K. Burke, *Phys. Rev. B - Condens. Matter Mater. Phys.*, 1996, **54**, 16533–16539.

16 C. Bannwarth, E. Caldeweyher, S. Ehlert, A. Hansen, P. Pracht, J. Seibert, S. Spicher and S. Grimme, *Wiley Interdiscip. Rev. Comput. Mol. Sci.*, 2021, **11**, 1–49.

17 J. D. Pack and H. J. Monkhorst, *Phys. Rev. B*, 1977, **16**, 1748–1949.

18 A. Kokalj, *J. Mol. Graph. Model.*, 1999, **17**, 176–179.

19 D. Upadhyay, B. Roondhe, A. Pratap and P. K. Jha, *Appl. Surf. Sci.*, 2019, **476**, 198–204.

20 B. Özdamar, G. Özbal, M. N. Çlnar, K. Sevim, G. Kurt, B. Kaya and H. Sevinçli, *Phys. Rev. B*, , DOI:10.1103/PhysRevB.98.045431.

21 A. Kanzariya, S. Vadalkar, S. K. Jana, L. K. Saini and P. K. Jha, *J. Phys. Chem. Solids*, 2024, **186**, 111799.

22 Y. Liu, C. Liu and A. Kumar, *Mol. Phys.*, , DOI:10.1080/00268976.2020.1798528.

23 S. Vadalkar, D. Chodvadiya, N. N. Som, K. N. Vyas and P. K. Jha, *ChemistrySelect*, 2023, **8**, e202204862.

24 R. K. Choudhury, B. R. Bhagat, K. H. Mali, R. Pokar and A. Dashora, *Appl. Surf. Sci.*, , DOI:10.1016/j.apsusc.2022.154426.

25 S. Peng, K. Cho, P. Qi and H. Dai, *Chem. Phys. Lett.*, 2004, **387**, 271–276.